A global assessment of the effects of solar farms on albedo, vegetation, and land surface temperature using remote sensing

Solar Energy 268 (2024) 112198

Contents lists available at ScienceDirect

Solar Energy

journal homepage: www.elsevier.com/locate/solener

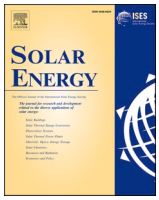

A global assessment of the effects of solar farms on albedo, vegetation, and land surface temperature using remote sensing

Zhengjie Xu [a,b], Yan Li [a,b,*], Yingzuo Qin [b,c], Eviatar Bach [d]

[a] State Key Laboratory of Earth Surface Processes and Resources Ecology, Beijing Normal University, Beijing, China
[b] Institute of Land Surface System and Sustainable Development, Faculty of Geographical Science, Beijing Normal University, Beijing, China
[c] School of Environmental Science and Engineering, Southern University of Science and Technology, Shenzhen, China
[d] Division of Geological and Planetary Sciences, California Institute of Technology, Pasadena, CA, USA

ARTICLE INFO

Keywords:
Solar farms
Photovoltaic power plants
Concentrating solar power plants
Albedo
Vegetation
Land surface temperature

ABSTRACT

The rapid development of solar energy worldwide has attracted increasing attention due to its climatic and environmental impacts. Using MODIS data, we quantified the effects of solar farms (SFs) on albedo, vegetation (using enhanced vegetation index (EVI) as a proxy), and land surface temperature (LST) based on 116 large SFs across the world. The results show that the installation of SFs decreased the annual mean surface shortwave albedo by 0.016 ± 0.009 (mean ± 1 STD) and reduced the EVI by 0.015 ± 0.019 relative to the surrounding areas. SFs produced a strong cooling effect of −0.49 ± 0.43 K in the annual mean land surface temperature during the daytime and a weaker cooling effect of −0.21 ± 0.25 K during the nighttime. The greatest impacts on albedo and daytime LST were observed in barren land, followed by grassland and cropland, while the opposite order applied for vegetation impact. In terms of seasonal and latitudinal variations, the largest impact was observed at high latitudes in winter on albedo, at mid-latitudes in summer on vegetation, and at low latitudes in spring–summer transitions on daytime LST. Correlation analysis showed that the albedo and LST impacts were enhanced over large SFs with high capacity. The vegetation and LST impacts were both correlated with geographic and climatic factors and dependent on the type of SF (photovoltaic or concentrating solar power). Our global assessment provides observational evidence for the effects of SF construction on the environment and local climate, which can help the sustainable development of solar energy.

1. Introduction

The development of solar energy serves as a key solution for energy transition to reduce carbon emissions and to address global warming [1]. As of 2019, the global electrical energy generated by solar power (including solar photovoltaic (PV) and thermal) was 694 Terawatt-hours (TWh, 1012 W-hours), accounting for approximately 10 % of total renewable energy [2]. By 2040, solar energy is projected to become one of the largest sources of renewable energy production worldwide, with power output from photovoltaic power plants (7200 TWh) exceeding hydropower, and together with wind power promoting the share of renewables to two-thirds of electricity generation [2]. Moreover, to achieve the Net Zero Emissions goal by 2050, solar energy needs rapid growth to more than 22 % of electricity generation by 2030 [3]. Despite the benefit of emission reduction [4], the deployment of solar energy through the construction of solar farms causes land cover changes, thereby affecting the surface energy balance (modifying roughness and albedo) [5], biodiversity (disturbing habitats) [6,7], and water resources (requiring water for cooling and cleaning) [8,9] these changes lead to climatic, ecological, and social consequences [10–14].

The construction and operation of solar farms (SFs), either using solar photovoltaic (PV) or concentrated solar power (CSP) technologies, have altered local surface properties and energy balance [15–17]. The impacts mainly manifest in changes to albedo and land surface temperature (LST) due to the combined effects of the dark surface of PV panels [18], electrical energy output [19], and heat transfer during power generation [20]. These impacts exhibit considerable regional variations and little consistency in the literature [21–23]. Field observational studies of a PV site in the Gobi Desert of China found that PV panels reduced daytime air temperature by 0.8 K during summer [24]

* Corresponding author at: Institute of Land Surface System and Sustainable Development, Faculty of Geographical Science, Beijing Normal University, Beijing 100875, China.
E-mail address: yanli.geo@gmail.com (Y. Li).

https://doi.org/10.1016/j.solener.2023.112198
Received 13 April 2023; Received in revised form 17 September 2023; Accepted 14 November 2023
Available online 5 January 2024

and decreased surface albedo by 0.14 compared to the reference area (with albedo of 0.23) [25]. However, other field observations in arid regions in California showed that the SF increased daytime air temperature up to 3 K and became a heat island [20]. A whole-year field experiment at a PV power plant in a desert area in western China indicated that PV panels increased soil temperature during winter but decreased it in other seasons, and the warming effect varied due to different installation methods of panels [26].

The impacts of solar farms on land surface properties and local climate also influence ecosystem processes and vegetation. However, the literature reports inconsistent results regarding the impacts of solar farms on local vegetation. It has been reported that the construction of SFs in California led to vegetation destruction and intensified desertification [27]. This is because a large natural land area was converted to harvest solar energy, which adversely affected natural ecosystems and biodiversity, especially in protected areas [10]. A field survey in California documented the negative effects of solar energy development on the desert scrub plant community by lowering perennial plant coverage [28]. In contrast, other scholars reported improved vegetation coverage and higher biomass and species richness in a PV plant in an arid region of China because the shading effect of PV panels reduced soil surface evaporation and alleviated water stress [29], and another study found that PV panels promoted biological soil crust development and vegetation growth, thus improving the soil texture and nutrition [30]. A study based on Landsat satellite data showed that the large-scale deployment of PV power stations promoted desert greening in the central part of northern China, primarily due to government-led photovoltaic desert control projects and favourable climatic change [31].

These considerable variations in the environmental impacts of SFs may arise from the heterogeneity of SF characteristics, such as their type (PV vs. CSP), spatial extent, capacity, installation methods [28], and background environmental conditions [29,32,33]. On the one hand, the impacts of SFs are scale-dependent because SFs with a larger size and higher capacity cause greater modifications to the land surface. In terms of climate impact, large SF (area $>$ 1000 ha) trigger more substantial impacts than small (area $<$ 100 ha) and medium-sized farms [20,22]. The climate impacts of continental-scale installations are not only local, as they affect regional and continental-scale climates [23,33,34]. On the other hand, the background conditions, e.g., underlying land cover types, influence the SF impacts on LST/air temperature [15,35], albedo [24] and vegetation cover [28,36,37]. For instance, PV panels installed on different land cover types exhibited varying impacts on albedo, leading to increased albedo on city rooftops but decreased albedo in desert regions [38]. The vegetation impacts also depend on how solar panels are deployed and on vegetation treatments. Ground-mounted PV panels clear vegetation on the ground, while halo treatment (plants within the solar field are roped off and left undisturbed) or bracket installations preserve vegetation [28,39]. Moreover, different solar energy technologies, such as PV and CSP, pose different risks to biodiversity. CSP is considered to be more damaging to species such as birds than PV because of the massive heat produced by the reflective mirrors [40].

The abovementioned SF impacts have been investigated by field observations from a single or few photovoltaic power plants [18,24,35] or through simulation by land surface and climate models [16,23,41]. Although in situ measurements provide valuable information on SF impacts, these measurements are usually only available at individual SFs and are insufficient to address spatial variations. Numerical simulations with land surface and climate models [38] reveal the dynamic interactions between installed SFs and the atmosphere, and their climatic impacts at a large scale [42–44]. However, uncertainties in models and parameterizations of SFs limit their capability to inform SF impacts at local scales. In comparison, satellite data with high spatial resolution and global coverage enables the detection of changes in surface properties (e.g., LST, vegetation, soil moisture) at fine scales. Widely available satellite data such as MODIS and Landsat with long temporal coverage can be used to identify the location of SFs and investigate their climate and environmental impacts [5,31,33,45].

However, existing studies on SF impacts using satellite data have mainly focused on individual or a few SFs [33,46]. The limited sampling has made the results less representative of SF impacts, with high heterogeneity. A global-scale study covering more SF from different regions and under different environmental conditions is necessary to address this issue. In this study, we analysed 116 solar farms across the world to provide a more comprehensive assessment of the SF impacts on albedo, vegetation, and land surface temperature. Specifically, we use long-term remote sensing observations from MODIS, which have good temporal coverage and moderate spatial resolutions, to investigate the SF effects on albedo, vegetation (as measured using EVI), and LST. Our goal is to deepen the understanding of renewable energy's environmental impacts and provide information for sustainable development.

2. Data and methods

2.1. Data

The SF site dataset was from Solar Wiki (*wiki-solar.org*, accessed July 2020). The dataset includes geographical location, construction year, and capacity for more than 1400 individual SFs with areas $\geq$ 95 ha around the world, covering both photovoltaic (PV) and concentrating solar power (CSP) sites. These sites were mainly located in China, the United States, Europe, and India. Since the spatial resolution of the MODIS data used was 1 km or finer, we selected 116 large SFs across the globe with a minimum occupying area of 400 ha (i.e., at least four 1-km pixels) to reduce the effect of mixed pixels. The underlying land cover type of each SF site was extracted from the 2009 MODIS land cover data (MCD12Q1 [47]) at a resolution of 1 km (Fig. 1a). The MODIS LST data product (MOD11A2 from Terra [48] and MYD11A2 from Aqua [49] with a 1-km spatial resolution and 8-day temporal resolution was used to quantify the local climate impact. The LST data included four local overpass times per day since 2002 (10:30 and 22:30 for Terra and 1:30 and 13:30 for Aqua). The MODIS albedo and enhanced vegetation index (EVI, a proxy for vegetation greenness) were applied to examine the effects of SF construction. The surface albedo data we used were from the MODIS MCD43A3 white-sky shortwave (0.3–5 μm) albedo product with a 500 m spatial resolution and daily temporal resolution [50]. The EVI dataset was the MYD13Q1 [51] and MOD13Q1 [52] 16-day product with a 250-m spatial resolution. Additionally, the 30-m digital elevation data were from the Shuttle Radar Topography Mission [53]. To explore factors influencing the spatial variations in SF impacts, we selected temperature and precipitation from Terra Climate data [54] at a spatial resolution of 1/24° and downwards shortwave radiation from ERA5 reanalysis data at 0.1° spatial resolution [55]. All these climate data were five-year mean values extracted at the solar farm area before construction. All the above data were obtained and processed on Google Earth Engine (https://code.earthengine.google.com/).

2.2. Quantifying SF impacts

To quantify the impacts of SFs on albedo, vegetation index, and land surface temperature, we compared the remotely sensed variable of interest between pixels inside and outside the SF while controlling for their different background conditions and natural climate variability. Specifically, the impacts of the SF were quantified as the differences in albedo, EVI, and LST between the SF location and adjacent non-SF buffer areas during a time window in which SF was built. The spatial boundary of each SF was manually delineated based on Google satellite imagery. The non-SF buffer areas were generated as the ring-shape area with a width of 1 km surrounding the SF and 1 km away from the boundary (Fig. 1 b, c, d). The 1-km distance was chosen because SF impacts are reportedly limited to $<$ 1 km (730 m) outside the SF boundary [56]. The non-SF buffering zone could be regarded as a natural condition free of SF impacts.

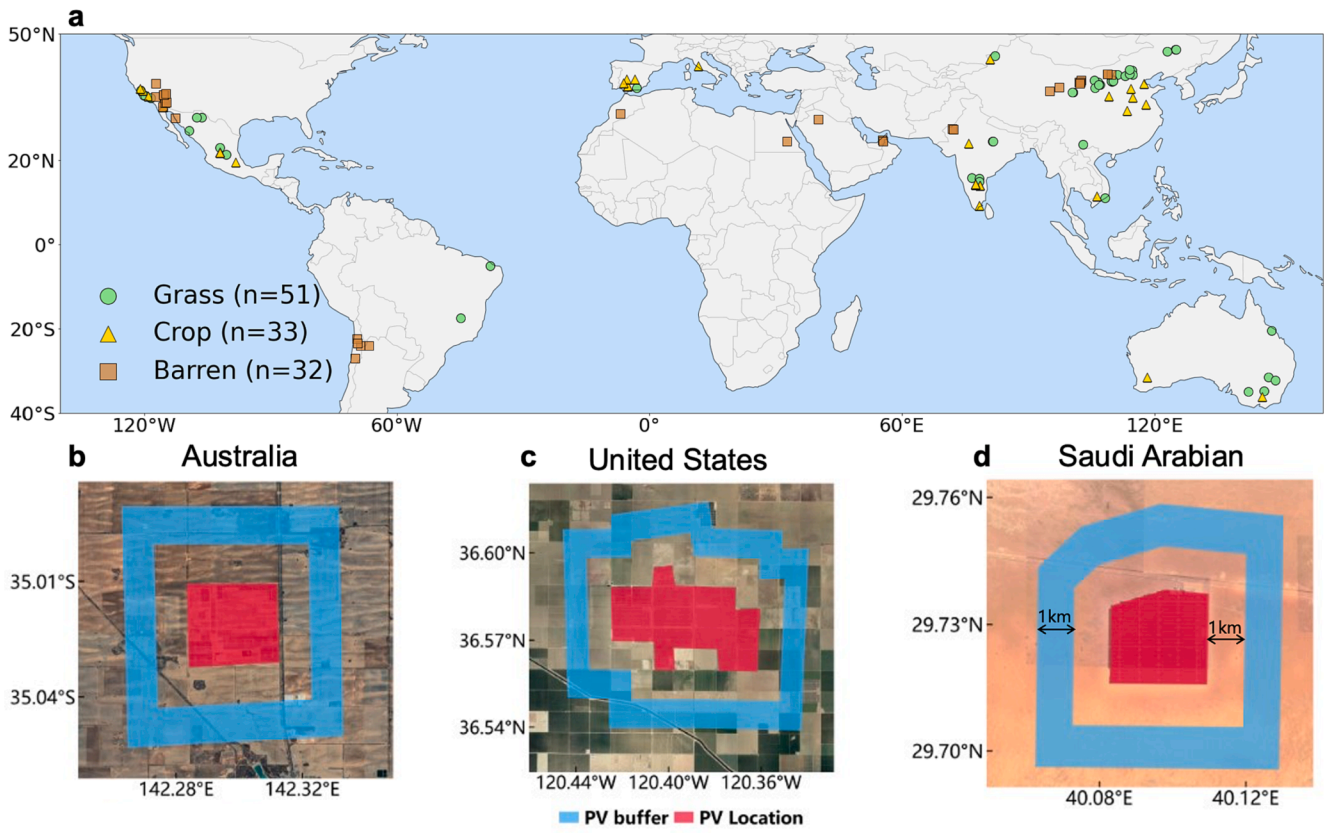

Fig. 1. The global distribution of 116 large SFs (a) and zoomed-in view for selected SFs (b-d). The locations of 116 SFs with areas > 400 ha and their land cover types are shown on the map. The three selected SFs (in red) and their buffering zones (in blue): an Australia PV power plant built in 2020 with an area of 652.8 ha located in grass (b), a United States PV site built in 2018 with an area of 1291.2 ha located in crops (c), and a Saudi Arabia PV site built in 2019 with an area of 653.3 ha located in barren land (d). (For interpretation of the references to colour in this figure legend, the reader is referred to the web version of this article.)

We describe our approach for quantifying the SF impact on LST (the impacts on albedo and EVI were estimated in the same way). SF impacts on LST (ΔLST) were quantified during a 5-year window (two years before and after the construction year), given by equation (1):

$$\Delta LST = \left(LST_{SF}^{after} - LST_{buffer}^{after}\right) - \left(LST_{SF}^{before} - LST_{buffer}^{before}\right) \quad (1)$$

where LST_{SF}^{before} and LST_{SF}^{after} are the 2-year averaged LSTs over the SF before and after SF construction, respectively. LST_{buffer}^{after} and LST_{buffer}^{before} are the 2-year averaged LSTs in non-SF buffering zones before and after construction, respectively. The rationale for this equation is that LST changes over the SF location contain effects from both SF and natural climate variability. In contrast, LST changes over the non-SF buffering zone are only affected by natural variability. Assuming that the SFs and their non-SF buffering zones in close distance share the same natural climate variability, subtracting these two can effectively remove natural climate variability and isolate the SF effect.

3. Results

3.1. Impacts of SF on albedo, EVI, and land surface temperature

3.1.1. Impacts on albedo

Fig. 2 shows the impacts of SFs on the annual mean surface shortwave albedo in different parts of the world. Globally, there was a significant decrease in albedo of −0.016 ± 0.009 (mean ± 1 STD) for most SF samples ($p < 0.001$, *t*-test). Regionally, SF in North America (NA) experienced a larger albedo decline (-0.014 ± 0.005 to −0.021 ± 0.017) than those in East and South Asia (ESA) (-0.010 ± 0.007 to −0.017 ± 0.010), possibly due to the larger capacity of SFs in NA (mean: 277 MW) than ESA (mean: 258 MW), or differences in the background albedo. When classifying SFs into different land cover types, the greatest albedo decreases were observed for SFs in barren lands (-0.025 ± 0.021), followed by grasslands (-0.014 ± 0.011) and croplands (-0.010 ± 0.007), consistent with previous research on Gobi desert [15] and cropland [36]. The largest albedo decrease (-0.088) was found for SFs on barren land in Arabia (as shown in Fig. 1d). The few SFs with albedo increases were mostly located in cropland (4 out of 7), with a maximum increase of 0.008.

3.1.2. Impacts on EVI

The vegetation impacts were quantified by comparing the difference in EVI between the SF and the non-SF buffering zones, representing land cover change impacts induced by SF on a broad scale (Fig. 3). Overall, the annual mean EVI decreased by −0.015 ± 0.019 ($p < 0.001$) across all SF samples, a −8.2 % reduction. A decrease in EVI was observed for 98 out of 116 samples. The EVI impacts exhibited clear regional variations and dependence on land cover types. All SF sites in North America showed a decreased EVI (0.023 ± 0.019). In contrast, approximately 1/3 of the SF sites in East and South Asia showed increased EVI. In terms of land cover type, in these two regions, SFs in cropland had a larger EVI decline (-19.09 % and −5.76 % for NA and ESA, respectively) than those in grassland (-6.60 % and −4.13 % for NA and ESA, respectively), and SFs in barren land had the weakest negative impact on EVI. However, in Europe and West Asia, SFs in barren land led to the greatest EVI reduction (-18.36 %). These results demonstrate a mixed sign of impacts of SFs on local vegetation.

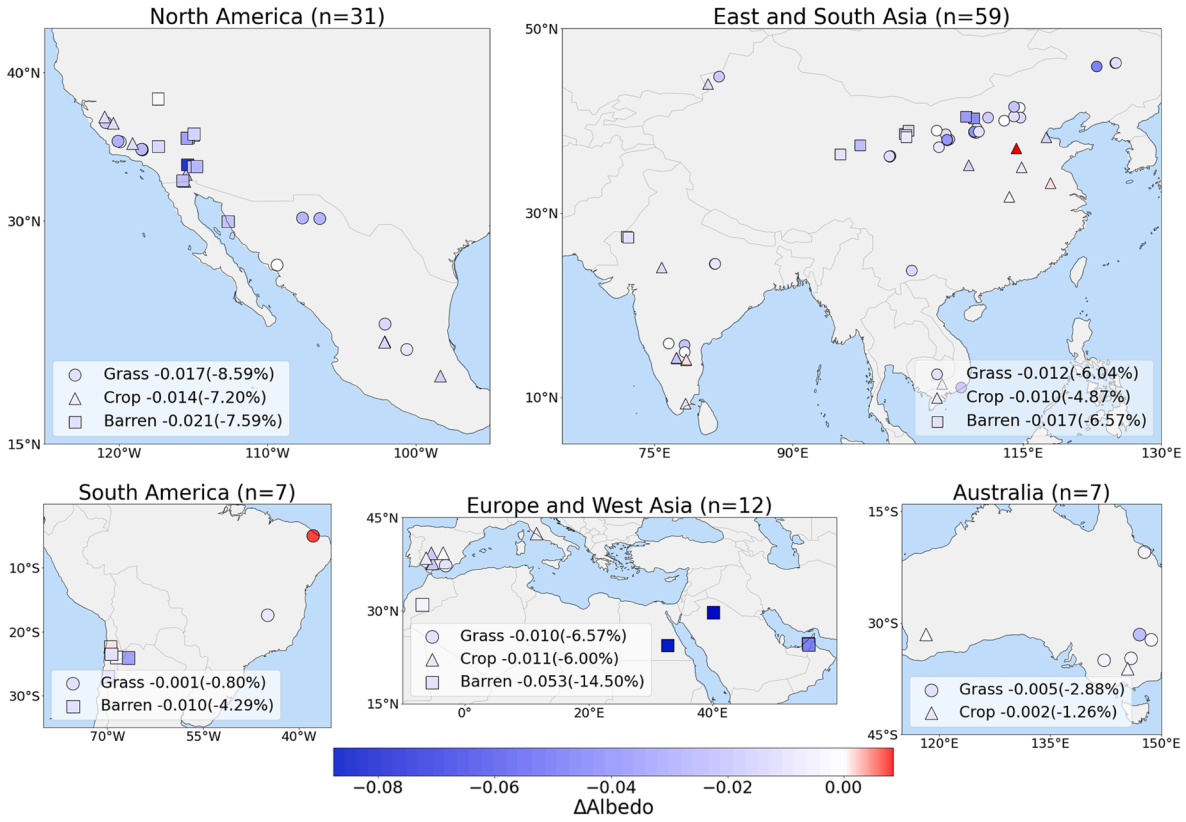

Fig. 2. Impacts of SFs on annual mean albedo in different regions. Red and blue denote the positive and negative effects of SF, respectively. Circles, triangles, and squares denote impacts classified into different land cover types. *n* represents the number of samples in the region. (For interpretation of the references to colour in this figure legend, the reader is referred to the web version of this article.)

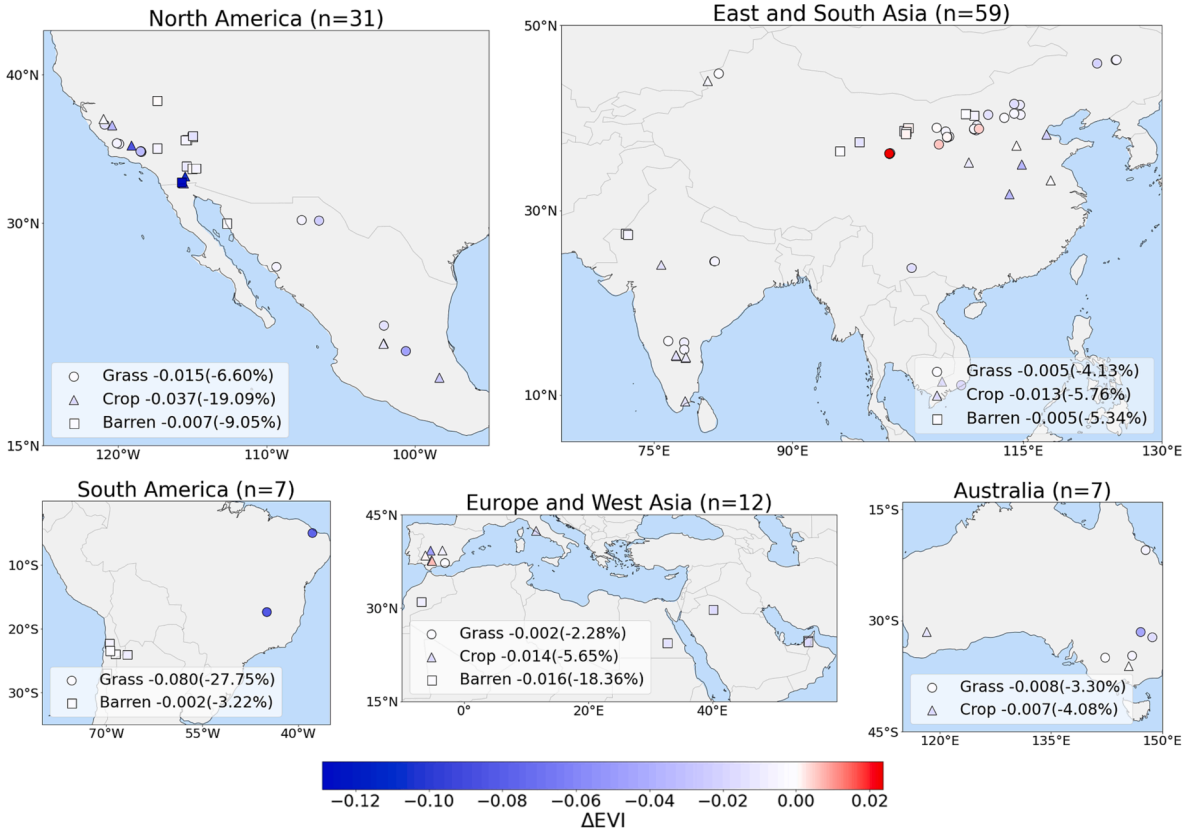

Fig. 3. Impacts of SFs on the annual mean EVI in different regions. Red and blue denote the positive and negative effects of SFs, respectively. Circles, triangles, and squares denote impacts classified into different land cover types. *n* represents the number of samples in the region. (For interpretation of the references to colour in this figure legend, the reader is referred to the web version of this article.)

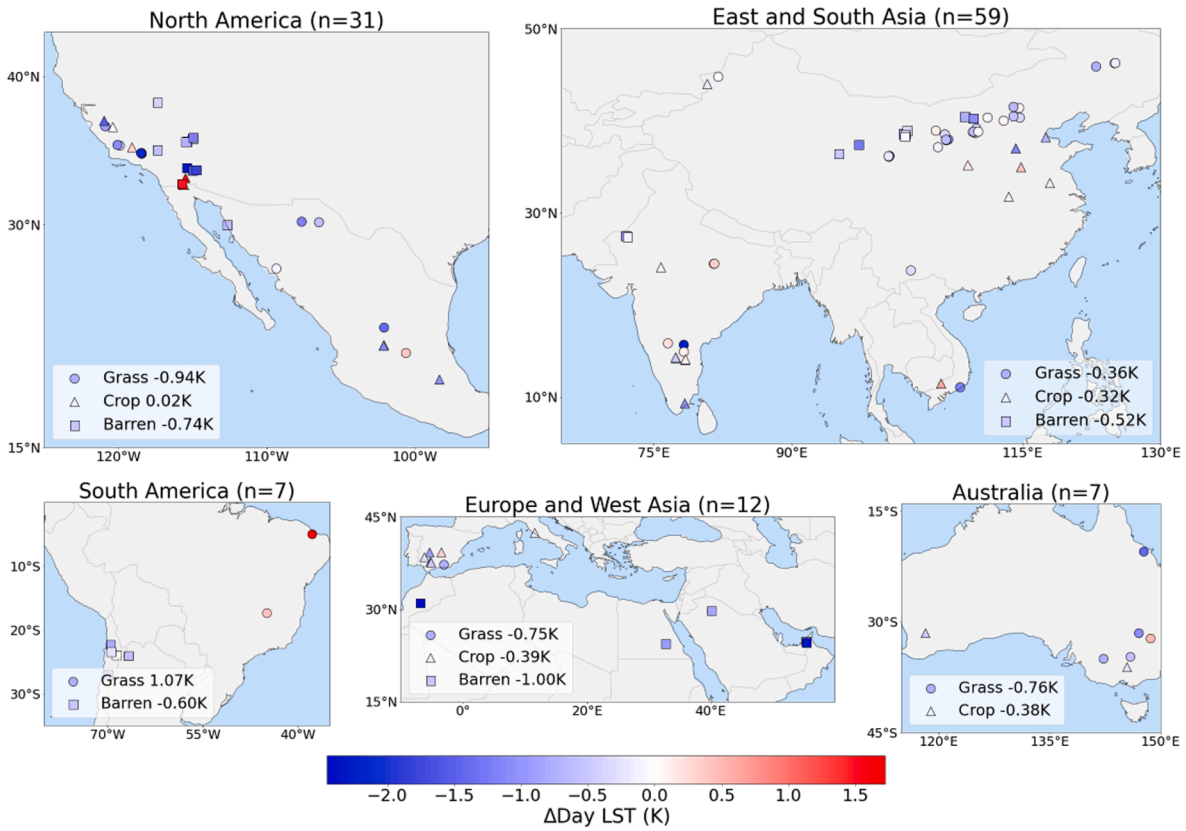

Fig. 4. Impacts of SFs on annual mean daytime LST in different regions. Red and blue denote the positive and negative effects of SFs, respectively. Circles, triangles, and squares denote impacts classified into different land cover types. *n* represents the number of samples in the region. (For interpretation of the references to colour in this figure legend, the reader is referred to the web version of this article.)

3.1.3. *Impacts on LST*

For the impacts of SFs on LST, we analysed LST data from the Aqua satellite because its local passing times (13:30 and 1:30) approximated the daytime maximum and nighttime minimum temperatures during a day. Fig. 4 and Fig. S1 show the impacts of SFs on the annual mean daytime and nighttime LSTs, respectively, in different regions. In general, SFs produced a stronger cooling impact on daytime LST than nighttime LST. During the daytime, cooling with a mean ΔLST of −0.49 ± 0.43 K ($p < 0.001$) was found in most (94 out of 116) SF samples (Fig. 4). The LST impacts varied across land cover types. During the daytime, SFs in barren land resulted in the largest cooling (-0.77 K ± 0.73 K), followed by grassland (-0.47 K), and the weakest cooling in cropland (-0.25 K). There were 22 SF samples showing warming effects in which cropland accounted for 45 % (10 out of 22).

The impacts of SFs on nighttime LST showed a weaker cooling and more heterogeneous pattern than daytime, with a mean ΔLST of −0.21 ± 0.25 K ($p < 0.001$) and a smaller percentage of sites experiencing cooling effect (82 out of 116) (Fig. S1). There were no consistent patterns in the nighttime LST impacts across different land cover types, as the impacts varied greatly both in sign and magnitude.

3.2. *The spatial-seasonal variations in SF impacts*

3.2.1. *Seasonal and latitudinal variations in SF impacts on albedo and EVI*

The reduction of albedo and EVI due to SFs were evident at the seasonal scale, but the strength varied across different latitudes (Fig. 5). At mid-latitudes (20-30°N), the albedo impact was strong throughout the year but slightly greater in November (-0.027 ± 0.015). The albedo impact transitioned from a stronger reduction in summer in temperate regions (30-35°N) to a larger impact in winter towards higher latitudes (>35°N). For ΔEVI, the largest impact was observed in spring and summer between 30°N and 35°N, a latitude band corresponding to the highest seasonality. This might be related to the dense vegetation in temperate regions, which was destroyed by SF construction [57]. At other latitudes, the EVI impacts were rather small without consistent seasonal patterns.

3.2.2. *Diurnal and seasonal variations in SF impacts on LST*

The MODIS LST data from Terra and Aqua combined provided four overpass times (1:30, 10:30, 13:30, and 22:30), which enabled exploration of the diurnal variations in LST impacts. The results in Fig. 6 show a conspicuous diurnal cycle in ΔLST across all sites. The cooling effect was smallest at midnight (-0.15 K at 1:30), and its magnitude increased in the morning (-0.44 K), peaked in the afternoon (-0.53 K), and decreased in the evening (-0.26 K). Such a diurnal cycle was most evident for SFs on barren land, having the largest diurnal range of 0.74 K (-0.07 to −0.81 K). The diurnal variations in ΔLST in grassland were also pronounced, ranging from −0.18 to −0.52 K. SFs on croplands showed the smallest diurnal variations in ΔLST, with slightly larger cooling in the daytime (-0.25 K) than in the nighttime (-0.21 K). The weak daytime cooling and small diurnal variations in cropland might be due to human activities such as irrigation. Irrigation-induced cooling in cropland around the SF could reduce the temperature contrast [58].

The SF impacts on LST also varied in different seasons and latitudes. By analysing the monthly and latitudinal patterns of the LST impacts, we found that the daytime cooling effect was stronger in winter (DJF) (-0.58 K) than in summer (JJA) (-0.47 K) in the Northern Hemisphere, especially from February to April (Fig. 7a). The magnitude of ΔLST peaked at 20-30°N (-0.75 K) and declined at high latitudes (>40°) (-0.29 K). The high latitudes also displayed little seasonality. Based on the latitudinal distribution of land cover types in Table 1, the peak daytime cooling at 20-30°N may be associated with the highest proportion of barren land (corresponding to the subtropical deserts), which intensified daytime cooling. During the nighttime, the cooling effect

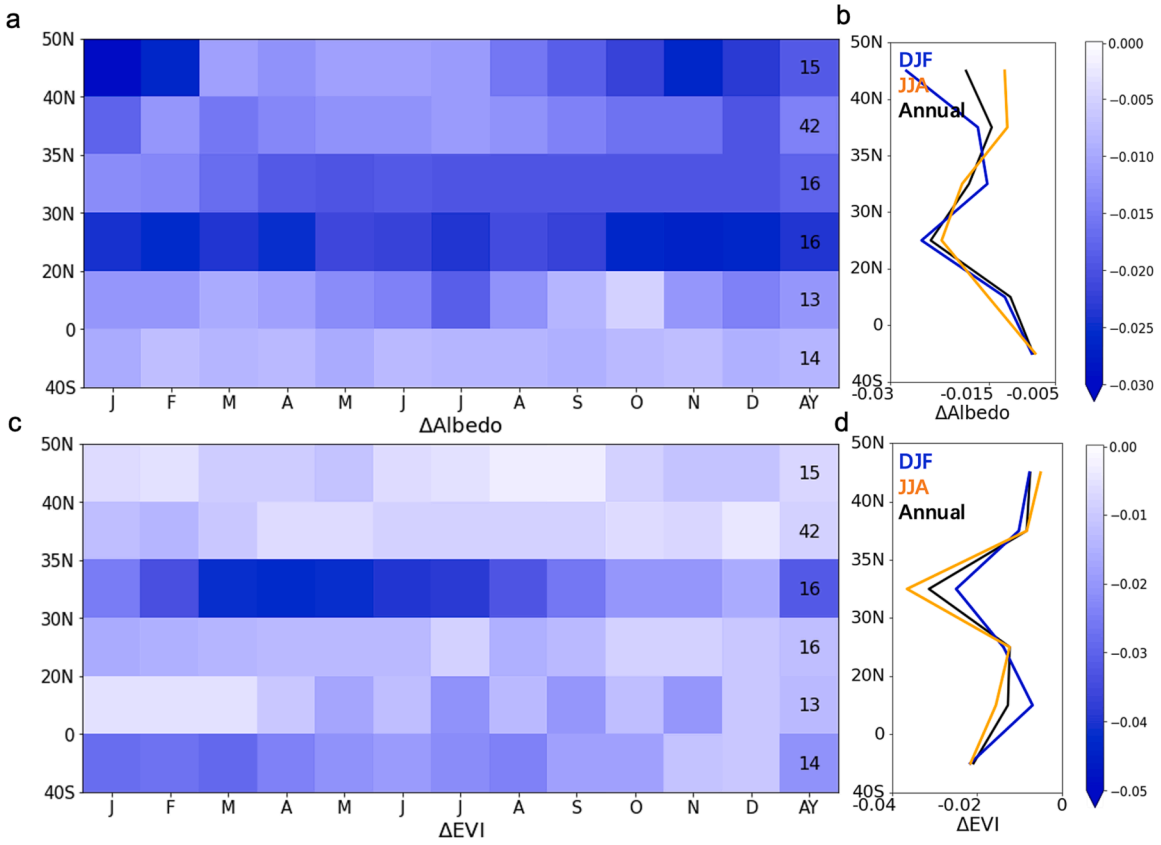

Fig. 5. Seasonal and latitudinal variations in SF impacts on albedo (a, b) and EVI (c, d). Each row and column represent the averaged impacts of a given month (*x*-axis) at a given latitude bands (*y*-axis). The last column represents the annual mean impact, and the number denotes the number of SF samples in each latitude band. The latitudinal patterns of ΔLST for summer (June to August (JJA)) and winter (December to February (DJF)) and the annual mean are shown in panels b and d.

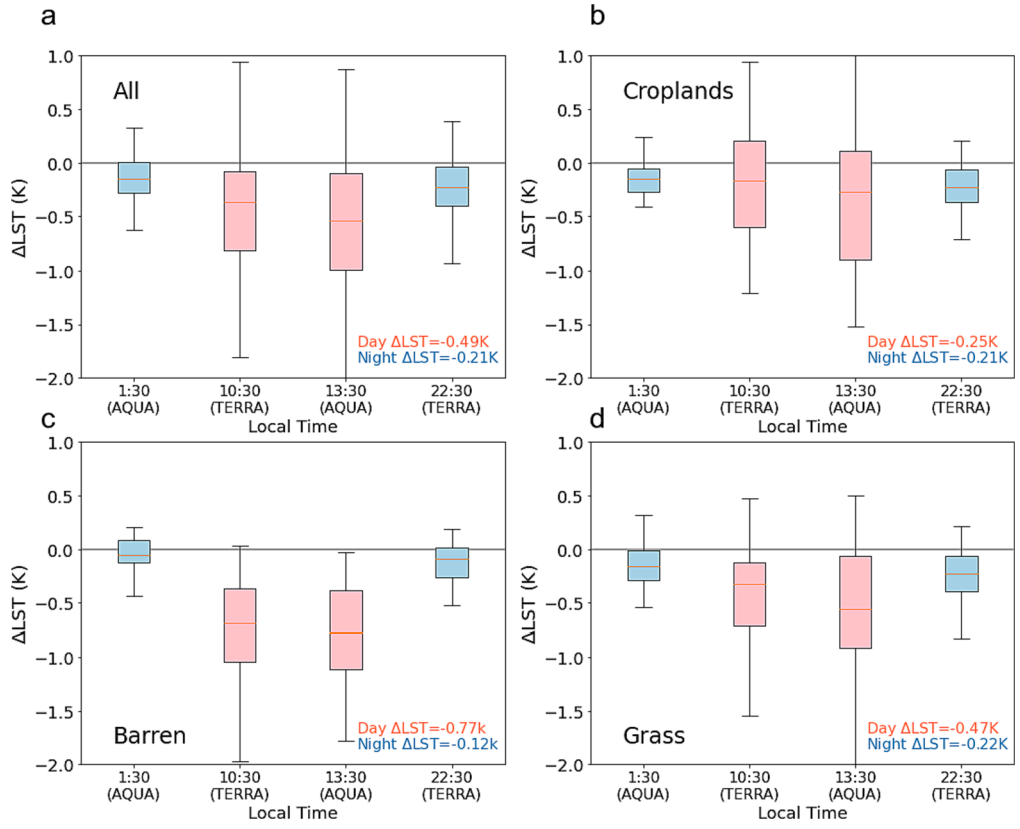

Fig. 6. Diurnal variations in LST impacts for all SF sites (a), croplands (b), barren lands (c), and grasslands (d). The diurnal variations in LST impact are estimated from four overpass times of MODIS Terra and Aqua LST data. Values on the lower right show the mean impact during daytime (red) and nighttime (blue). (For interpretation of the references to colour in this figure legend, the reader is referred to the web version of this article.)

exhibited a much weaker seasonality but a pronounced decreasing trend towards higher latitudes. In addition, there was occasionally abrupt warming (in November in the high latitude band 40°N-50°N) and cooling (in September at latitude band 0-20°N). Further inspection showed that these abrupt effects were caused by a few (1–2) anomalous samples; therefore, we suspect these outliers are due to data noise.

3.3. Correlation analysis for spatial variations in SF impacts and drivers

To better understand the drivers of the spatial variations in SF impacts, we collected multiple possible influencing factors and calculated their correlations with annual mean SF impacts (Fig. 8a). These factors include those related to solar farms, such as installed capacity and construction area, geographical factors such as latitude and altitude, and climatic factors, such as precipitation, air temperature, and downwards shortwave solar radiation. These climatic factors were five-year mean values extracted at the solar farm area before construction. ΔAlbedo only significantly correlated with the capacity (r = -0.19, $p < 0.05$) and area (r = -0.17, $p < 0.05$), indicating that larger SFs led to a greater reduction in albedo than smaller farms. ΔEVI was positively correlated with latitude (r = 0.21, $p < 0.05$) but negatively correlated with air temperature (r = -0.23, $p < 0.05$), solar radiation (r = -0.25, $p < 0.05$), and EVI (-0.20, $p < 0.05$). The vegetation reduction decreased at higher latitudes, and it was minimal for SFs in the hot desert with strong solar radiation (Fig. 3). These results suggest that vegetation change was closely linked to environmental factors. For ΔLST, similar to albedo, SFs with large capacity were more likely to produce a greater cooling effect in both daytime (r = -0.21, $p < 0.05$) and nighttime (r = -0.26, $p < 0.05$).

Table 1
Distribution of land cover types at SF sites in different latitudinal bands.

Latitudinal band	Samples number	Crop	Barren	Grass
40–50 N	15	2 (13 %)	3 (20 %)	10 (67 %)
35–40 N	42	11 (26 %)	12 (29 %)	19 (45 %)
30–35 N	16	6 (38 %)	5 (31 %)	5 (31 %)
20–30 N	16	3 (19 %)	7 (44 %)	6 (38 %)
0–20 N	13	9 (69 %)	0 (0 %)	4 (31 %)
0-40S	14	2 (14 %)	5 (36 %)	7 (50 %)

However, latitude, altitude, precipitation and EVI had opposite effects on daytime and nighttime LSTs, which implied different dominant factors between day and night. For example, more precipitation during daytime decreases solar radiation, inhibiting electricity conversion and the resultant LST cooling effects (r = 0.23, $p < 0.05$). In contrast, more precipitation at night increases soil moisture, slowing down the environmental radiative cooling processes, enhancing LST differences (r = -0.29, $p < 0.05$).

Correlation analysis suggested that the SF impacts themselves were interconnected with each other (Fig. 8b). ΔAlbedo was positively correlated with daytime ΔLST (r = 0.46, $p < 0.05$) and ΔEVI (r = 0.36, $p < 0.05$), indicating that albedo changes may contribute to ΔLST through their effect on surface energy balance and photovoltaic conversion process. The decline in vegetation may also in turn amplify the albedo impact. However, the nonsignificant correlation between ΔAlbedo and nighttime ΔLST (r = 0.16, $p > 0.05$), as well as the significant positive correlation between nighttime ΔLST and daytime ΔLST (r = 0.26, $p < 0.05$), again implied that the mechanisms responsible for the cooling

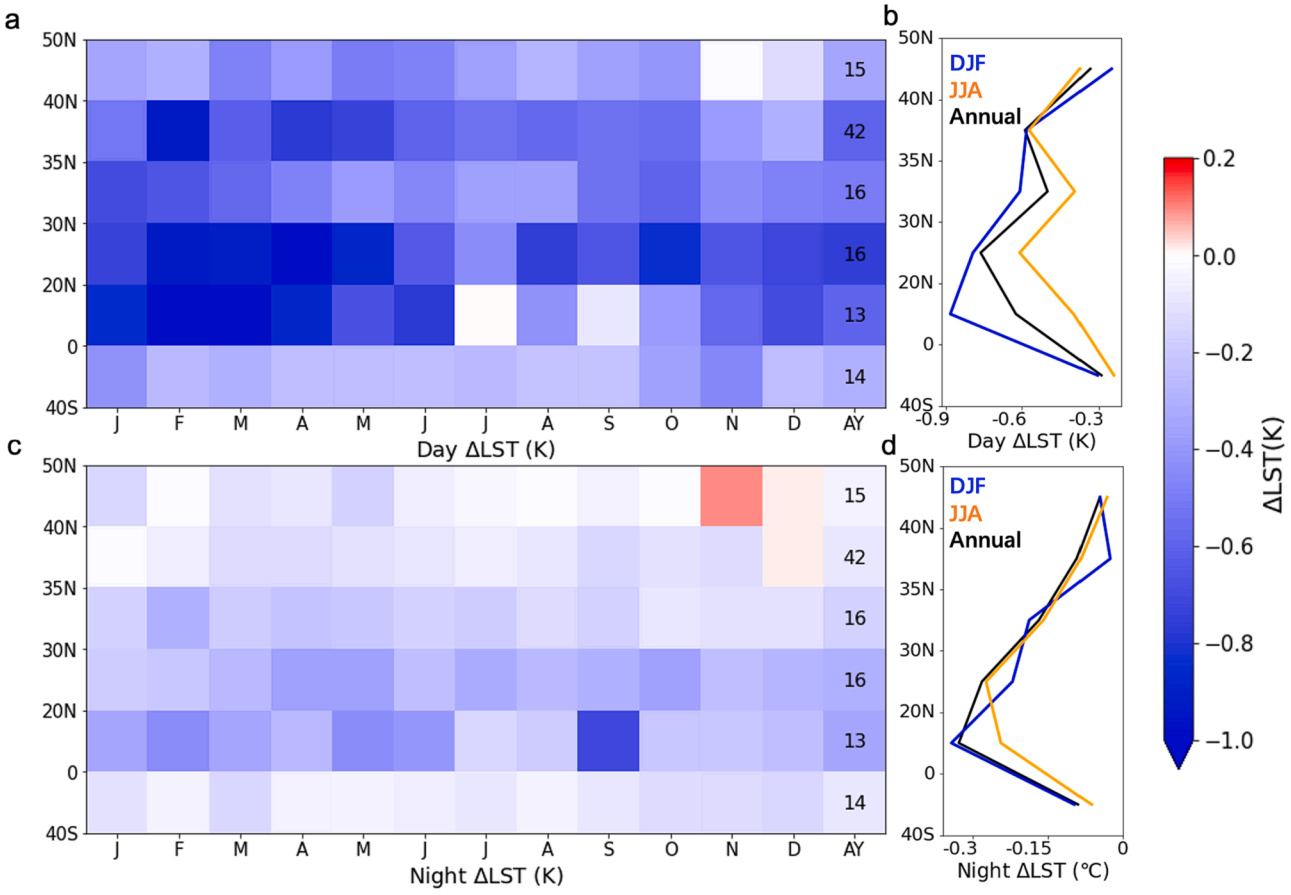

Fig. 7. Seasonal and latitudinal variations in SF impacts on daytime (a, b) and nighttime LSTs (c, d). Each row and column represent the averaged impacts of a given month (x-axis) at a given latitude band (y-axis). The last column represents the annual mean impact, and the number denotes the number of SF samples in each latitude band. The latitudinal patterns of ΔLST for summer (June to August (JJA)) and winter (December to February (DJF)) and the annual mean are shown in panels b and d.

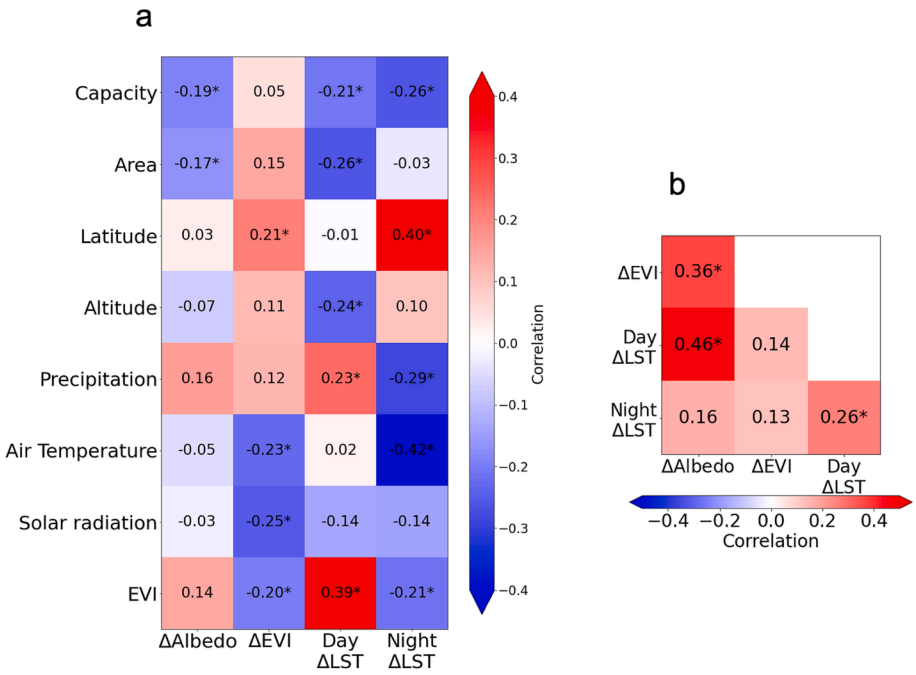

Fig. 8. The correlation between influencing factors (a) and SF impacts (b). Influencing factors included the installed capacity, construction area, latitude, altitude, precipitation, air temperature (2 m), downwards solar radiation, and EVI. SF impacts on albedo (ΔAlbedo), EVI (ΔEVI) and LST (day ΔLST and night ΔLST). Numbers with asterisks indicate statistical significance ($p < 0.05$) by t test.

during daytime and nighttime were different but also somewhat connected. Daytime cooling might be attributed to the effective albedo effect (albedo corrected for electricity conversion, a greater value than the original albedo; see [22]) and shadow effects, while night cooling could result from the daytime cooling and the thermal inertia of the land surface. Furthermore, due to the high thermal conductivity of solar panels, they may cool more quickly at night compared to their surroundings [35,59].

Since many correlations were tested at once, it may lead the problem of multiple comparisons, which increases the probability of getting a p-value < 0.05 just by chance. To account for multiple comparisons, the significance of the correlations was tested using the Benjamini–Hochberg procedure [60], with a false discovery control level $\alpha = 0.1$. At the significance level of 0.1, all the same correlations we found to be significant are still significant, and no others, which showed that the correlations above were quite robust.

4. Discussion

Our study, based on 116 SFs worldwide, provides a more comprehensive assessment of SF impacts compared to earlier studies that focused on one or a small number of sites. Our results indicated that the impacts of SFs were complex and variable. Both SF characteristics and environmental factors were key drivers of spatial–temporal variability of the SF impacts, but there was still large unexplained variability that requires further investigation of other factors not considered here.

For albedo impacts, because the reflection efficiency of PV panels in the shortwave band is lower than that of most land cover types [61], a decreased albedo was observed at most SF sites. However, some SF sites, mostly in cropland, showed increased albedo (Fig. 2), probably caused by their dark soil having lower albedo than PV panels [36]. The seasonality of the albedo impacts increased with latitude (Fig. 5a), possibly due to larger seasonal changes in solar radiation and surface snow at high latitudes. The strong albedo decrease in winter at high latitudes might be related to frequent snow, which increases the albedo contrast when the non-SF buffering zones are covered by highly reflective snow while the cleaning of SF modules can prevent them from being covered by snow.

For vegetation impacts, the decreased vegetation is mainly caused by the construction of the SFs, which may remove the original vegetation and damage vegetation growth at the site [28]. However, vegetation recovery in SF sites was reported in the arid area of China (Fig. 3), which could be due to the ecological protection and restoration carried out during the construction of SFs [31,57,62]. Additionally, increased vegetation in SF sites could be caused by changing microclimate and microhabitat conditions induced by the SFs. Previous studies have shown that PV panels significantly increased total aboveground productivity and plant species diversity in grasslands [63] since SFs reduce wind velocity [64] and lower evapotranspiration (ET) and drought stress in arid sandy ecosystems [29,65]. Moreover, the operation of large PV facilities usually consumes water for cooling and cleaning, providing extra moisture for underlying vegetation. Although both positive and negative vegetation effects were reported by past studies for individual SF sites, our study indicated that the construction and operation of most SFs had a negative impact on vegetation if no protective interventions were taken. With proper system design, the negative vegetation effects could be mitigated or even reversed. For example, agrivoltaics, by combining photovoltaic panels and agricultural activities, utilize the shading effect of PV panels and irrigation measures to improve vegetation growth [66,67], and they fully use the vertical space for both crop production and power generation [32,68]. This reveals the importance of human management on the vegetation impacts of SFs.

Another complication comes from the limitation of remote sensing in detecting changes in vegetation covered by PV panels. The decreased vegetation signal was obtained from the differences in the surface reflectance spectral features between SF facilities (such as photovoltaic panels) and surrounding vegetation, which can be interpreted as land cover change impacts on a broader scale. However, the unique spectral properties of solar panels may also influence the retrieval of vegetation index, which depends on certain optical band information (red, green, blue, near-infrared) designed originally for natural vegetation, thus introducing uncertainties to the detection of vegetation effect. Moreover, opaque PV panels could interfere with this vegetation signal because vegetation under the panels could not be directly “seen” by

satellite. Therefore, our results are not informative about the impact of solar panels on plants under the panels at micro scales; field survey or *in situ* experiments are needed to investigate this question, and satellite-derived vegetation indexes tailored for applications on solar panels could greatly improve the capability of remote sensing in detecting the vegetation impact of solar farms at large scale.

For LST impacts, our results showed an overall strong cooling in daytime LST (-0.49 K) and weak cooling in nighttime LST (-0.21 K) at SF sites. However, these impacts exhibited considerable spatial–temporal variability, probably reflecting the heterogeneity in SF characteristics and environmental conditions. Despite the cooling for the majority of sites, 22 SF samples on grassland (11), cropland (10) and barren land (1) showed daytime warming, with a mean magnitude of 0.50 K. There were 34 samples on barren land (14), grassland (13), and cropland (7) that showed nighttime warming, with an average of 0.11 K. Excluding SF samples with warming led to a much larger daytime cooling effect (-0.77 K) but not much difference in the nighttime cooling (-0.25 K). The SF effect on daytime LST was mainly caused by the photovoltaic process. Photovoltaic generation changes the surface reflectance of radiation by converting solar energy into electrical output (approximately 10 % to 15 % of the absorbed solar energy is converted to electricity). The removed energy from the surface energy budget could result in surface cooling. As a result, although the apparent albedo of the PV panel decreases, the effective albedo (which includes the portion converted to electricity) tends to increase significantly [22]. The cooling effect due to this energy conversion is limited to the PV area and the time duration of power generation [69]. Therefore, the area and capacity of SF were strongly correlated with the daytime LST effect (Fig. 8a). For most SF panels, the optimal temperature to achieve maximum photovoltaic conversion efficiency is approximately 26 °C [69]. We suspect that an environmental temperature closer to this optimal value will have a higher photovoltaic conversion efficiency, which might create a stronger cooling effect. This might partially explain the seasonality and latitudinal variations in the LST effect shown in Fig. 7, since SF at middle and low latitudes may enter this optimal temperature range in spring, and the sites at high latitudes may enter it in summer. The nighttime LST effect may be due to the daytime cooling and thermal inertia. Furthermore, it could be related to the different thermal conductivities of solar panels and the background land surface [19]. Compared with most land surfaces, solar panels have higher thermal conductivity, so that their surface temperature drops faster at night. Barren land surfaces, mostly consisting of sand and rock, also have high thermal conductivity. This explains why SF over barren land had a smaller nighttime LST effect than other land cover types.

It should be noted that the effects of SF on surface temperature and near-surface air temperature are not consistent [70]. Some studies have noted that PV panels have a significant heating effect on air temperature within 2–5 m of the surface, which creates a heat island effect [17,71]. This is because the PV panels generate very high sensible heat during their operation, which directly heats up the air above the PV surface. It has been reported that urban rooftop PV increases sensible heat flux by 10 times during the daytime, which warms the atmosphere [72]. In summary, PV panels capture the energy originally absorbed and dissipated directly by the ground surface, and convert it into electrical energy output while releasing heat. PV changes both the local surface energy balance and microclimates, with different effects on LST and near-surface air temperature.

Since there are different types of solar energy technologies, PV and CSP, we searched for pairs of PV and CSP SFs with the same land cover and in the same latitudinal band (Fig. 5) to compare their impacts. As shown in Table 2, on barren land, PV had overall stronger impacts than CSP, except for a larger daytime cooling with CSP. In contrast, on cropland, PV had weaker impacts on albedo and daytime LST than CSP but greater impacts on EVI and night LST. CSP's stronger daytime LST effect might be related to its higher conversion efficiency. The energy conversion efficiency of CSP (30 %-40 %) is generally higher than that of PV (20 %) [73], which means that more energy would be harvested by CSP than by PV. However, at night, the thermal energy storage technology to maintain CSP all-day operation becomes a heat source [74], which may slow the temperature drop produced by its higher thermal conductivity than the environment. The different impacts on albedo and EVI between PV and CSP might be related to their specific installation methods. The comparison should be interpreted with caution because of the small size of paired samples and the potentially different siting and environmental conditions among pairs. Further research comparing CSP and PV from the same SF site could avoid the confounding factors in our study and make a fairer comparison.

Our method for quantifying SF impacts has uncertainties and limitations. First, due to the constraint of spatial resolution and data quality, the MODIS data used in this study were insufficient to cover small SF samples, which introduced uncertainty to the quantification. Although we focused on SF covering a large area, mixed pixel problems were still present. To reduce the uncertainty from a specific dataset, we used the MODIS data from both Aqua and Terra satellites for LST (Aqua: MYD11A2, Terra: MOD11A2) and EVI (Aqua: MYD13Q1, Terra: MOD13Q1). Our main findings are broadly consistent between these datasets. Moreover, the different local passing times of Aqua and Terra allowed us to analyse the diurnal variation in LST impacts. Another data limitation is that the retrieval algorithms of MODIS LST data are not optimized for solar panels since parameters like emissivity still come from natural vegetation without considering solar panel as a different land cover type. The smaller emissivity of solar panels (~0.8) than natural vegetation (>0.9), if accounted for, would lead to a smaller daytime cooling effect [5]. This emphasizes the need to develop optimized satellite data products with higher spatial resolutions (such as Landsat) to better quantify the local impacts of SFs, especially for smaller ones.

Second, as described in the Methods, we applied a 5-year time window (2 years before and after the construction year) to estimate ΔLST, ΔAlbedo, and ΔEVI between the SF and buffering area. The choice of window length may influence the results. We thus compared results based on different window time lengths (Table 3). Although the available sample numbers differed across different time windows, the results were essentially the same except for ΔEVI. The ΔEVI is lessened for the

Table 2
Comparison of annual mean impacts between photovoltaic (PV) and concentrated solar power (CSP) solar farms.

Impacts of SF	Type of SF Barren CSP (n[a] = 4)	Similar* PV (n = 8)	All PV (n = 28)	Cropland CSP (n = 4)	Similar PV (n = 13)	All PV (n = 29)	Grass PV (n = 51)	All samples (n = 116)
ΔAlbedo	−0.011	−0.026	−0.027	−0.014	−0.011	−0.010	−0.016	−0.016
ΔEVI	−0.004	−0.023	−0.012	−0.018	−0.040	−0.025	−0.013	−0.015
Day ΔLST	−1.28 K	−0.85 K	−0.73 K	−0.56 K	−0.22 K	−0.22 K	−0.47 K	−0.49 K
Night ΔLST	−0.01 K	−0.18 K	−0.15 K	−0.01 K	−0.13 K	−0.23 K	−0.22 K	−0.21 K

* *Similar PV* refers to PV sites which have the same land cover type and are within the same latitudinal band (defined in Fig. 5) as CSP. *All PV* refers to PV sites which have the same land cover type as CSP.

[a] The n in the table indicates the number of samples.

Table 3
Sensitivity analysis of SF impacts to different time windows.

Impacts of SF	Time window length		
	3 years (n^a = 139)	5 years (n = 116)	7 years (n = 64)
ΔAlbedo	−0.015	−0.016	−0.017
ΔEVI	−0.023	−0.015	−0.017
ΔDay LST	−0.53 K	−0.49 K	−0.48 K
ΔNight LST	−0.20 K	−0.21 K	−0.21 K

We reported results based on a 5-year time window length in the main text.
[a] The n in the table indicates the number of samples.

5- and 7-year windows compared to the 3-year window, possibly due to the vegetation being given more time to recover after the SF construction. Our choice of the 5-year time window was to balance the number of available SF samples, because longer time windows would filter out samples whose construction years were close to the beginning or end of the study period, and shorter time windows would make the results more sensitive to interannual variations.

Third, a buffering zone to represent background environmental conditions is critical when quantifying SF impacts. We created a buffer zone 1 km from the SF to reduce the spillover effect (changes in land surface at one location affecting adjacent areas) from areas too close to the SF [56]. Further research is needed to determine how to select a more appropriate reference condition for SFs.

Fourth, for simplicity, we assigned a single construction year for every SF site. The construction of a large SF, however, may last several years and could have long-term signals. In addition, SF information from Solar-Wiki may also have uncertainty, and not all SFs are included in the data. More recent global datasets, for example, those identified by machine learning [75], can be a supplement to provide additional information about SF.

5. Conclusion

Based on satellite remote sensing data, our assessment of 116 SF around the world provided new observational evidence for the impacts of SF on albedo, vegetation, and land surface temperature. Our results revealed significant land surface cooling, especially during the daytime, and a mostly negative impact on albedo and vegetation. The large spatial–temporal heterogeneity in these impacts highlighted the role of SF characteristics, environmental factors, and other local factors not considered here. Our attempts to quantify SF impacts demonstrated the great potential of satellite remote sensing for investigating various SF impacts, and the proposed methodology can be applied to other regions with available SF information. For this purpose, it would be essential to promote the development of satellite data products optimized for solar farm-related variables (e.g., with refined retrieval algorithms or parameters) to improve the usability and robustness of satellite data for solar farm-related applications. Further studies could utilize such satellite data to better characterize fine-scale impacts (with spatial resolutions higher than MODIS data such as Landsat) and expand the scope to address other ecological and environmental impacts. These satellite-derived findings could be combined with field observations and numerical simulations to clarify the mechanism of SF impacts. In-depth knowledge of SF impacts is informative about the environmental consequences of solar energy development and can help guide the planning of renewable energy to meet both climate targets and sustainable development.

6. Data availability

Code and data of this study will be available at Figshare (https://doi.org/10.6084/m9.figshare.24152766).

CRediT authorship contribution statement

Zhengjie Xu: Methodology, Software, Data curation, Writing – original draft. **Yan Li:** Conceptualization, Resources, Writing – review & editing. **Yingzuo Qin:** Methodology, Writing – review & editing. **Eviatar Bach:** Methodology, Writing – review & editing.

Declaration of competing interest

The authors declare that they have no known competing financial interests or personal relationships that could have appeared to influence the work reported in this paper.

Acknowledgments

This research is funded by the National Natural Science Foundation of China (No. 41901115) and the Fundamental Research Funds for the Central Universities.

Appendix A. Supplementary data

Supplementary data to this article can be found online at https://doi.org/10.1016/j.solener.2023.112198.

References

[1] V. Masson, M. Bonhomme, J.L. Salagnac, X. Briottet, A. Lemonsu, Solar panels reduce both global warming and urban heat island, Front. Environ. Sci. 2 (2014) 14, https://doi.org/10.3389/fenvs.2014.00014.
[2] IEA, Renewables – World Energy Outlook 2019 – Analysis - IEA, (2019). https://www.iea.org/reports/world-energy-outlook-2019/renewables (accessed September 26, 2022).
[3] IEA, Renewable Power – Analysis - IEA, (2021). https://www.iea.org/reports/renewable-power (accessed September 5, 2022).
[4] Z. Zhang, M. Chen, T. Zhong, R. Zhu, Z. Qian, F. Zhang, Y. Yang, K. Zhang, P. Santi, K. Wang, Y. Pu, L. Tian, G. Lü, J. Yan, Carbon mitigation potential afforded by rooftop photovoltaic in China, Nat. Commun. 14 (2023) 2347, https://doi.org/10.1038/s41467-023-38079-3.
[5] C. Fan, X. Huang, Direct impact of solar farm deployment on surface longwave radiation, Environ. Res. Commun. 3 (2021), 125006, https://doi.org/10.1088/2515-7620/ac40f1.
[6] L.J. Sonter, M.C. Dade, J.E.M. Watson, R.K. Valenta, Renewable energy production will exacerbate mining threats to biodiversity, Nat. Commun. 11 (2020) 1–6, https://doi.org/10.1038/s41467-020-17928-5.
[7] D. Serrano, A. Margalida, J.M. Pérez-García, J. Juste, J. Traba, F. Valera, M. Carrete, J. Aihartza, J. Real, S. Mañosa, C. Flaquer, I. Garin, M.B. Morales, J. T. Alcalde, B. Arroyo, J.A. Sánchez-Zapata, G. Blanco, J.J. Negro, J.L. Tella, C. Ibañez, J.L. Tellería, F. Hiraldo, J.A. Donázar, Renewables in Spain threaten biodiversity, Science 370 (2020) 1182–1183, https://doi.org/10.1126/science.abf6509.
[8] T. Tsoutsos, N. Frantzeskaki, V. Gekas, Environmental impacts from the solar energy technologies, Energy Policy 33 (2005) 289–296, https://doi.org/10.1016/S0301-4215(03)00241-6.
[9] C. Wu, H. Liu, Y. Yu, W. Zhao, J. Liu, H. Yu, O. Yetemen, Ecohydrological effects of photovoltaic solar farms on soil microclimates and moisture regimes in arid Northwest China: A modeling study, Sci. Total Environ. 802 (2022), 149946, https://doi.org/10.1016/j.scitotenv.2021.149946.
[10] R.R. Hernandez, M.K. Hoffacker, M.L. Murphy-Mariscal, G.C. Wu, M.F. Allen, Solar energy development impacts on land cover change and protected areas, Proc. Nat. Acad. Sci. USA 112 (2015) 13579–13584, https://doi.org/10.1073/pnas.1517656112.
[11] V.C. Bleich, C.M. Aiello, C.W. Epps, J.D. Wehausen, Green energy projects at odds with conservation, Science 380 (2023) 1021, https://doi.org/10.1126/science.adi0761.
[12] C. Wu, H. Liu, Y. Yu, W. Zhao, L. Guo, J. Liu, O. Yetemen, Ecohydrological insight: Solar farms facilitate carbon sink enhancement in drylands, J. Environ. Manage. 342 (2023), 118304, https://doi.org/10.1016/j.jenvman.2023.118304.
[13] Y. Zhang, Z. Tian, B. Liu, S. Chen, J. Wu, Effects of photovoltaic power station construction on terrestrial ecosystems: A meta-analysis, accessed June 19, 2023, Front. Ecol. Evol. 11 (2023), https://www.frontiersin.org/articles/10.3389/fevo.2023.1151182.
[14] C.E. Pavlowsky, T. Gliedt, Individual and local scale interactions and adaptations to wind energy development: A case study of Oklahoma, USA, Geogr. Sustain. 2 (2021) 175–181, https://doi.org/10.1016/j.geosus.2021.08.003.
[15] R. Chang, Y. Shen, Y. Luo, B. Wang, Z. Yang, P. Guo, Observed surface radiation and temperature impacts from the large-scale deployment of photovoltaics in the barren area of Gonghe, China, Renew. Energy 118 (2018) 131–137, https://doi.org/10.1016/j.renene.2017.11.007.

[16] R. Chang, Y. Yan, Y. Luo, C. Xiao, C. Wu, J. Jiang, W. Shi, A coupled WRF-PV mesoscale model simulating the near-surface climate of utility-scale photovoltaic plants, Sol. Energy 245 (2022) 278–289, https://doi.org/10.1016/j.solener.2022.09.023.
[17] A.M. Broadbent, E.S. Krayenhoff, M. Georgescu, D.J. Sailor, The Observed Effects of Utility-Scale Photovoltaics on Near-Surface Air Temperature and Energy Balance, J. Appl. Meteorol. Climatol. 58 (2019) 989–1006, https://doi.org/10.1175/JAMC-D-18-0271.1.
[18] Y. Hua, J. Chai, L. Chen, P. Liu, The Influences of the Desert Photovoltaic Power Station on Local Climate and Environment: A Case Study in Dunhuang Photovoltaic Industrial Park, Dunhuang City, China in 2019, Atmosphere 2022, Vol. 13, Page 1235. 13 (2022) 1235. https://doi.org/10.3390/ATMOS13081235.
[19] S. Rehman, I. El-Amin, Performance evaluation of an off-grid photovoltaic system in Saudi Arabia, Energy 46 (2012) 451–458, https://doi.org/10.1016/J.ENERGY.2012.08.004.
[20] G.A. Barron-Gafford, R.L. Minor, N.A. Allen, A.D. Cronin, A.E. Brooks, M.A. Pavao-Zuckerman, The photovoltaic heat island effect: Larger solar power plants increase local temperatures, Sci. Rep. 6 (2016) 1–7, https://doi.org/10.1038/srep35070.
[21] D. Millstein, S. Menon, Regional climate consequences of large-scale cool roof and photovoltaic array deployment, Environ. Res. Lett. 6 (2011), 034001, https://doi.org/10.1088/1748-9326/6/3/034001.
[22] H. Taha, The potential for air-temperature impact from large-scale deployment of solar photovoltaic arrays in urban areas, Sol. Energy 91 (2013) 358–367, https://doi.org/10.1016/j.solener.2012.09.014.
[23] A. Hu, S. Levis, G.A. Meehl, W. Han, W.M. Washington, K.W. Oleson, B.J. Van Ruijven, M. He, W.G. Strand, Impact of solar panels on global climate, Nat. Clim. Change 6 (2016) 290–294, https://doi.org/10.1038/nclimate2843.
[24] X. Gao, L. Yang, X. Hou, X. Hui, The local climate impact of photovoltaic solar farms - Results from a field observation campaign in gobi desert, in: 2017: pp. 1397–1408. https://doi.org/10.18086/swc.2017.22.01.
[25] Z. Li, Y. Zhao, Y. Luo, L. Yang, P. Li, X. Jin, J. Jiang, R. Liu, X. Gao, A comparative study on the surface radiation characteristics of photovoltaic power plant in the Gobi desert, Renew. Energy 182 (2022) 764–771, https://doi.org/10.1016/J.RENENE.2021.10.054.
[26] S. Yue, M. Guo, P. Zou, W. Wu, X. Zhou, Effects of photovoltaic panels on soil temperature and moisture in desert areas, Environ. Sci. Pollut. Res. 28 (2021) 17506–17518, https://doi.org/10.1007/S11356-020-11742-8/TABLES/6.
[27] T.D. Allison, T.L. Root, P.C. Frumhoff, Thinking globally and siting locally – renewable energy and biodiversity in a rapidly warming world, Clim. Change 126 (2014) 1–6, https://doi.org/10.1007/s10584-014-1127-y.
[28] S.M. Grodsky, R.R. Hernandez, Reduced ecosystem services of desert plants from ground-mounted solar energy development, Nat. Sustain. 3 (2020) 1036–1043, https://doi.org/10.1038/s41893-020-0574-x.
[29] Y. Liu, R. Zhang, Z. Huang, Z. Cheng, M. López-Vicente, X. Ma, G. Wu, Solar photovoltaic panels significantly promote vegetation recovery by modifying the soil surface microhabitats in an arid sandy ecosystem, Land Degrad. Dev. 30 (2019) 2177–2186, https://doi.org/10.1002/ldr.3408.
[30] L. Luo, Y. Zhuang, H. Liu, W. Zhao, J. Chen, W. Du, X. Gao, Environmental impacts of photovoltaic power plants in northwest China, Sustain. Energy Technol. Assess. 56 (2023), 103120, https://doi.org/10.1016/j.seta.2023.103120.
[31] Z. Xia, Y. Li, W. Zhang, R. Chen, S. Guo, P. Zhang, P. Du, Solar photovoltaic program helps turn deserts green in China: Evidence from satellite monitoring, J. Environ. Manage. 324 (2022), 116338, https://doi.org/10.1016/j.jenvman.2022.116338.
[32] C. Dupraz, H. Marrou, G. Talbot, L. Dufour, A. Nogier, Y. Ferard, Combining solar photovoltaic panels and food crops for optimising land use: Towards new agrivoltaic schemes, Renew. Energy 36 (2011) 2725–2732, https://doi.org/10.1016/j.renene.2011.03.005.
[33] X. Zhang, M. Xu, Assessing the Effects of Photovoltaic Powerplants on Surface Temperature Using Remote Sensing Techniques, Remote Sens. (Basel) 12 (2020) 1825, https://doi.org/10.3390/rs12111825.
[34] Y. Li, E. Kalnay, S. Motesharrei, J. Rivas, F. Kucharski, D. Kirk-Davidoff, E. Bach, N. Zeng, Climate model shows large-scale wind and solar farms in the Sahara increase rain and vegetation, Science 361 (2018) 1019–1022, https://doi.org/10.1126/science.aar5629.
[35] W. Wu, S. Yue, X. Zhou, M. Guo, J. Wang, L. Ren, B. Yuan, Observational study on the impact of large-scale photovoltaic development in deserts on local air temperature and humidity, Sustainability (Switzerland) 12 (2020) 3403, https://doi.org/10.3390/SU12083403.
[36] E.H. Adeh, S.P. Good, M. Calaf, C.W. Higgins, Solar PV power potential is greatest over croplands, Sci. Rep. 9 (2019), https://doi.org/10.1038/s41598-019-47803-3.
[37] Y. Liu, R.Q. Zhang, X.R. Ma, G.L. Wu, Combined ecological and economic benefits of the solar photovoltaic industry in arid sandy ecosystems, J. Clean. Prod. 262 (2020), 121376, https://doi.org/10.1016/j.jclepro.2020.121376.
[38] S. Li, J. Weigand, The potential for climate impacts from widespread deployment of utility-scale solar energy installations: an environmental remote sensing perspective, J. Remote Sens. GIS 06 (2017), https://doi.org/10.4172/2469-4134.1000190.
[39] J. Macknick, B. Beatty, G. Hill, Overview of Opportunities for Co-Location of Solar Energy Technologies and Vegetation, (2013). https://doi.org/10.2172/1115798.
[40] S. Pfenninger, P. Gauché, J. Lilliestam, K. Damerau, F. Wagner, A. Patt, Potential for concentrating solar power to provide baseload and dispatchable power, Nat. Clim. Change 4 (2014) 689–692, https://doi.org/10.1038/nclimate2276.
[41] J. Heusinger, A.M. Broadbent, D.J. Sailor, M. Georgescu, Introduction, evaluation and application of an energy balance model for photovoltaic modules, Sol. Energy 195 (2020) 382–395, https://doi.org/10.1016/j.solener.2019.11.041.
[42] A. Lovins, Energy Strategy: The Road Not Taken, Rocky Mountain Institute. 55 (1976) 65–96. https://rmi.org/insight/energy-strategy-the-road-not-taken/ (accessed January 4, 2021).
[43] R.R. Hernandez, S.B. Easter, M.L. Murphy-Mariscal, F.T. Maestre, M. Tavassoli, E. B. Allen, C.W. Barrows, J. Belnap, R. Ochoa-Hueso, S. Ravi, M.F. Allen, Environmental impacts of utility-scale solar energy, Renew. Sustain. Energy Rev. 29 (2014) 766–779, https://doi.org/10.1016/j.rser.2013.08.041.
[44] E. Kabir, P. Kumar, S. Kumar, A.A. Adelodun, K.H. Kim, Solar energy: Potential and future prospects, Renew. Sustain. Energy Rev. 82 (2018) 894–900, https://doi.org/10.1016/J.RSER.2017.09.094.
[45] Z. Xia, Y. Li, R. Chen, D. Sengupta, X. Guo, B. Xiong, Y. Niu, Mapping the rapid development of photovoltaic power stations in northwestern China using remote sensing, Energy Rep. 8 (2022) 4117–4127, https://doi.org/10.1016/J.EGYR.2022.03.039.
[46] M.M. Edalat, Remote sensing of the environmental impacts of utility-scale solar energy plants, UNLV Theses, Dissertations, Professional Papers, and Capstones. (2017) 8–9. https://doi.org/10.34917/11156717.
[47] M. Friedl, D. Sulla-Menashe, MCD12Q1 MODIS/Terra+Aqua Land Cover Type Yearly L3 Global 500m SIN Grid V006, (2019). https://doi.org/10.5067/MODIS/MCD12Q1.006.
[48] Z. Wan, S. Hook, G. Hulley, MOD11A2 MODIS/Terra Land Surface Temperature/Emissivity 8-Day L3 Global 1km SIN Grid V006, (2015). https://doi.org/10.5067/MODIS/MOD11A2.006.
[49] Z. Wan, S. Hook, G. Hulley, MYD11A2 MODIS/Aqua Land Surface Temperature/Emissivity 8-Day L3 Global 1km SIN Grid V006, (2015). https://doi.org/10.5067/MODIS/MYD11A2.006.
[50] C. Schaaf, Z. Wang, MCD43A3 MODIS/Terra+Aqua BRDF/Albedo Daily L3 Global - 500m V006, (2015). https://doi.org/10.5067/MODIS/MCD43A3.006.
[51] K. Didan, MYD13Q1 MODIS/Aqua Vegetation Indices 16-Day L3 Global 250m SIN Grid V006, (2015). https://doi.org/10.5067/MODIS/MYD13Q1.006.
[52] K. Didan, MOD13Q1 MODIS/Terra Vegetation Indices 16-Day L3 Global 250m SIN Grid V006, (2015). https://doi.org/10.5067/MODIS/MOD13Q1.006.
[53] A. Jarvis, E. Guevara, H.I. Reuter, A.D. Nelson, Hole-filled SRTM for the globe : version 4 : data grid, (2008). https://research.utwente.nl/en/publications/hole-filled-srtm-for-the-globe-version-4-data-grid (accessed November 24, 2022).
[54] J.T. Abatzoglou, S.Z. Dobrowski, S.A. Parks, K.C. Hegewisch, TerraClimate, a high-resolution global dataset of monthly climate and climatic water balance from 1958–2015, Sci. Data 5 (2018), 170191, https://doi.org/10.1038/sdata.2017.191.
[55] Muñoz Sabater, J, ERA5-Land monthly averaged data from 1950 to present, (2019). https://doi.org/10.24381/cds.68d2bb30.
[56] G. Li, R.R. Hernandez, G.A. Blackburn, G. Davies, M. Hunt, J.D. Whyatt, A. Armstrong, Ground-mounted photovoltaic solar parks promote land surface cool islands in arid ecosystems, Renew. Sustain. Energy Trans. (2021), 100008, https://doi.org/10.1016/J.RSET.2021.100008.
[57] J. Vervloesem, E. Marcheggiani, M.A.M. Choudhury, B. Muys, Effects of photovoltaic solar farms on microclimate and vegetation diversity, Sustainability. 14 (2022) 7493, https://doi.org/10.3390/su14127493.
[58] Y. Li, K. Guan, B. Peng, T.E. Franz, B. Wardlow, M. Pan, Quantifying irrigation cooling benefits to maize yield in the US Midwest, Glob. Chang. Biol. 26 (2020) 3065–3078, https://doi.org/10.1111/gcb.15002.
[59] S. Yue, W. Wu, X. Zhou, L. Ren, J. Wang, The Influence of Photovoltaic Panels on Soil Temperature in the Gonghe Desert Area, Environ. Eng. Sci. 38 (2021) 910–920, https://doi.org/10.1089/ees.2021.0014.
[60] Y. Benjamini, Y. Hochberg, Controlling the false discovery rate: a practical and powerful approach to multiple testing, J. Royal Stat. Soc. Seri. (Methodological) 57 (1995) 289–300, https://doi.org/10.1111/j.2517-6161.1995.tb02031.x.
[61] C. Fan, X. Huang, Satellite-observed changes of surface spectral reflectances due to solar farming and the implication for radiation budget, Environ. Res. Lett. 15 (2020), 114047, https://doi.org/10.1088/1748-9326/abbdea.
[62] Z. Liu, T. Peng, S. Ma, C. Qi, Y. Song, C. Zhang, K. Li, N. Gao, M. Pu, X. Wang, Y. Bi, X. Na, Potential benefits and risks of solar photovoltaic power plants on arid and semi-arid ecosystems: an assessment of soil microbial and plant communities, accessed August 28, 2023, Front. Microbiol. 14 (2023), https://www.frontiersin.org/articles/10.3389/fmicb.2023.1190650.
[63] Z. Bai, A. Jia, Z. Bai, S. Qu, M. Zhang, L. Kong, R. Sun, M. Wang, Photovoltaic panels have altered grassland plant biodiversity and soil microbial diversity, accessed December 19, 2022, Front. Microbiol. 13 (2022), https://www.frontiersin.org/articles/10.3389/fmicb.2022.1065899.
[64] J. Jiang, X. Gao, B. Chen, The Impact of Utility-Scale Photovoltaics Plant on Near Surface Turbulence Characteristics in Gobi Areas, Atmos. 12 (2021) 18, https://doi.org/10.3390/atmos12010018.
[65] R. Chang, Y. Yan, J. Wu, Y. Wang, X. Gao, Projected PV plants in China's Gobi Deserts would result in lower evaporation and wind, Sol. Energy 256 (2023) 140–150, https://doi.org/10.1016/j.solener.2023.04.003.
[66] H. Dinesh, J.M. Pearce, The potential of agrivoltaic systems, Renew. Sustain. Energy Rev. 54 (2016) 299–308, https://doi.org/10.1016/j.rser.2015.10.024.
[67] E. Hassanpour Adeh, J.S. Selker, C.W. Higgins, Remarkable agrivoltaic influence on soil moisture, micrometeorology and water-use efficiency, PLoS One 13 (2018) e0203256.
[68] H. Marrou, L. Guilioni, L. Dufour, C. Dupraz, J. Wery, Microclimate under agrivoltaic systems: Is crop growth rate affected in the partial shade of solar panels? Agric. For. Meteorol. 177 (2013) 117–132, https://doi.org/10.1016/j.agrformet.2013.04.012.
[69] A.R. Amelia, Y.M. Irwan, W.Z. Leow, M. Irwanto, I. Safwati, M. Zhafarina, Investigation of the effect temperature on photovoltaic (PV) panel output

performance, Int. J. Adv. Sci. Eng. Inform. Technol. 6 (2016) 682–688, https://doi.org/10.18517/IJASEIT.6.5.938.
[70] J. Jiang, X. Gao, Q. Lv, Z. Li, P. Li, Observed impacts of utility-scale photovoltaic plant on local air temperature and energy partitioning in the barren areas, Renew. Energy (2021), https://doi.org/10.1016/j.renene.2021.03.148.
[71] W.D. Solecki, C. Rosenzweig, L. Parshall, G. Pope, M. Clark, J. Cox, M. Wiencke, Mitigation of the heat island effect in urban New Jersey, Environ. Hazards 6 (2005) 39–49, https://doi.org/10.1016/j.hazards.2004.12.002.
[72] K.E. Brown, A. Baniassadi, J.V. Pham, D.J. Sailor, P.E. Phelan, Effects of rooftop photovoltaics on building cooling demand and sensible heat flux into the environment for an installation on a white roof, ASME J. Eng. Sustain. Build. Cities 1 (2020), https://doi.org/10.1115/1.4046399.
[73] IRENA, Renewable power generation costs in 2021, International Renewable Energy Agency, Abu Dhabi, 2021.
[74] Y. Zhao, A. Dunn, J. Lin, D. Shi, Chapter 13 - Photothermal Effect of Nanomaterials for Efficient Energy Applications, in: X. Wang, X. Chen (Eds.), Novel Nanomaterials for Biomedical, Environmental and Energy Applications, Elsevier, 2019, pp. 415–434, https://doi.org/10.1016/B978-0-12-814497-8.00013-8.
[75] L. Kruitwagen, K.T. Story, J. Friedrich, L. Byers, S. Skillman, C. Hepburn, A global inventory of photovoltaic solar energy generating units, Nature 598 (2021) 604–610, https://doi.org/10.1038/s41586-021-03957-7.